Clinical Radiology xxx (xxxx) xxx

Contents lists available at ScienceDirect

Clinical Radiology

journal homepage: www.clinicalradiologyonline.net

MRI features of extraocular muscle metastases compared to those of other extraocular muscle diseases of non-thyroid origin

A. Miura [a], N. Kashiwagi [b,*], M. Sakai [b], T. Hyodo [c], H. Takahashi [a], Y. Miyauchi [d], O. Maenishi [e], K. Ishii [c], K. Nakanishi [b], N. Tomiyama [a]

[a] *Department of Radiology, Osaka University Graduate School of Medicine, Suita, Osaka, 565-0871, Japan*
[b] *Department of Diagnostic and Interventional Radiology, Osaka International Cancer Institute, Osaka-city, Osaka, 541-8567, Japan*
[c] *Department of Radiology, Kindai University Faculty of Medicine, Osakasayama, Osaka, 589-8511, Japan*
[d] *Department of Radiology, Sakai City Medical Center, Sakai, Osaka, 593-8304, Japan*
[e] *Department of Pathology, Kindai University Faculty of Medicine, Osakasayama, Osaka, 589-8511, Japan*

ARTICLE INFORMATION

Article history:
Received 29 March 2022
Received in revised form
7 August 2022
Accepted 30 August 2022

AIM: To identify the magnetic resonance imaging (MRI) features of metastases to the extraocular muscles (EOM metastases).

MATERIAL AND METHODS: The MRI features of 19 patients with EOM metastases were compared with those of 24 patients with EOM diseases of non-thyroid origin. MRI was used to assess the number of tumours, morphology, signal intensity on T2-weighted images, enhancement patterns, and apparent diffusion coefficient (ADC) values.

RESULTS: Single muscular involvement was observed in 10 patients, and multiple muscular involvement was observed in nine patients. The morphology was focally discrete in nine patients, and diffuse infiltrative in 10 patients; all the nine patients with focal discrete morphology presented with single muscular lesions. On T2-weighted images, the signal intensities were intermediate or low in 15 patients and a mixture of high and intermediate in four patients. In 14 patients for whom contrast-enhanced images were available, ring enhancement (n=5), heterogeneous diffuse enhancement (n=5), and homogeneous enhancement (n=4) were seen. The mean ADC value was 0.98 $\times$ 10^{-3} mm^2/s. Compared to other EOM diseases of non-thyroid origin, single muscular presentation, focal discrete morphology, the presence of hyperintensity on T2-weighted images, and ring or heterogeneous enhancement were significantly more frequent in EOM metastases.

CONCLUSION: The MRI features of EOM metastases showed two main patterns: a single discrete mass and multiple infiltrative masses. In addition to the presentation as a single discrete mass, the presence of hyperintensity on T2-weighted images and ring or heterogeneous enhancement can aid in the differentiation of EOM metastases from other EOM diseases.

* Guarantor and correspondent: N. Kashiwagi, Department of Diagnostic and Interventional Radiology, Osaka International Cancer Institute, Osaka-city, Osaka, 541-8567, Japan.
E-mail address: n-kashiwagi@radiol.med.osaka-u.ac.jp (N. Kashiwagi).

https://doi.org/10.1016/j.crad.2022.08.148
0009-9260/

Introduction

Although thyroid-associated orbitopathy is the most common cause of extraocular muscle (EOM) enlargement, accounting for 95% of these cases, a variety of other diseases can cause EOM enlargement.[1] EOM metastases account for 18–23% of the EOM enlargement cases with non-thyroid origin.[1–3]

EOM metastases usually occur during advanced malignant disease,[3–6] but 13% of EOM metastases cases initially present as an occult malignancy.[4] In addition, the presenting symptoms and signs are non-specific,[2–4] which requires a comprehensive understanding of their imaging features. Only a few studies and small case series have reported imaging features for EOM metastases[7,8] because of its relative rarity.[9–12] The present study reports the magnetic resonance imaging (MRI) features of EOM metastases in 19 patients with a brief description of their clinical features. In addition, MRI features of EOM metastases were compared to those of other diseases causing EOM enlargement. Thyroid-associated orbitopathy was excluded from the comparison, because it is usually diagnosed by a combination of clinical and laboratory findings,[13,14] indicating that MRI features are not necessarily important for its differential diagnosis.

Materials and methods

The review committee approved this retrospective study (reference no. 19428) and waived the requirement for informed consent.

Patients

By assessing the medical records retrospectively of three referral centres for cancer in Japan between January 2009 and January 2021, 19 patients diagnosed with EOM metastases were identified. The patients included two men and 17 women, with a mean age of 59.4 years (range: 20–82 years). The diagnoses of EOM metastases were made by histological examination in seven patients; the remaining 12 patients were diagnosed based on the following clinical features: (1) presence of an EOM mass on MRI, (2) presence of malignancies that had already developed distant metastases to other organs, and (3) no clinical features suggestive of hyperthyroidism except for proptosis.

As a control group, 24 patients were identified who had other diseases of non-thyroidal origin that caused EOM enlargement during the same period at one of the three centres. The control group comprised 15 men and nine women, with a mean age of 66.0 years (range: 41–87 years). In 20 of these patients, the diagnoses were made by a combination of clinical features and histopathological examination, including 12 lymphomas, five immunoglobulin G4-related diseases (IgG4-RD), two idiopathic orbital inflammatory diseases, and one granulomatosis with polyangiitis. The remaining four patients were diagnosed using clinical features based mainly on the responses to steroid therapy, which included three cases of idiopathic orbital inflammatory diseases, and one case of IgG4-RD.

MRI protocol

MRI examinations were performed using a 1.5 T magnet in six patients and a 3 T magnet in 13 patients. In the pre-contrast axial plane, T1-weighted images (repetition time [TR])/echo time [TE]: 279–840/2.3–20 ms) and axial T2-weighted images (TR/TE: 2,500–6,000/80–261 ms) were obtained for all patients. Fat-suppressed T2-weighted images (TR/TE: 3,909–5,800/83–112 ms), including short inversion time inversion recovery (STIR) sequences (TR/TE: 2,500–8,000/45–109 ms, inversion time: 140–210 ms), were obtained in 13 patients, and diffusion-weighted (DW) images (b factors: 0 and 1,000 s/mm^2) were obtained in 10 patients. The apparent diffusion coefficient (ADC) maps were constructed automatically from the DW images. On coronal planes, fat-suppressed T2-weighted images or STIR images were obtained in 11 patients, and T1-weighted images with or without the fat-suppression technique were obtained in 11 patients. Contrast-enhanced T1-weighted imaging, with or without a fat-suppression technique, was performed in 14 patients. Axial and coronal images were obtained in all patients, and sagittal images were obtained in 11 patients. The section thickness ranged from 3–5 mm, and the pixel size ranged from 0.35 × 0.35 to 0.86 × 0.86 mm.

Clinical data extraction

In addition to the baseline characteristics of the 19 patients with EOM metastases, the following clinical features of EOM metastases were collected: primary tumour, time interval from primary diagnosis to EOM metastases, symptoms associated with EOM metastases, the presence of metastases to other organs, and the presence of metastases to other skeletal muscles.

Image assessment

Three diagnostic radiologists participated in the image assessment process. Two of the radiologists (with 5 and 22 years of experience in neuroradiology) reviewed all MRI images independently, blinded to the clinical information. Differences between the two readers were resolved by the third radiologist, with 23 years of experience, whose reading was taken as the final result.

The evaluated items included the number of tumours (single or multiple), laterality (unilateral or bilateral), involved muscles, tumour morphology, signal intensities (T1-weighted images, T2-weighted images, and fat-suppressed T2-weighted images), enhancement patterns (homogeneous, heterogeneous, ring enhancement), and mean ADC values on DW images. The largest lesion was evaluated when multiple EOM metastases were present. Using the criteria of previous studies,[7,15] the morphology was divided into two types: focal discrete or diffuse infiltrative. The focal discrete type was defined as a tumour with a well-defined focal intramuscular mass showing ovoid or

Please cite this article as: Miura A et al., MRI features of extraocular muscle metastases compared to those of other extraocular muscle diseases of non-thyroid origin, Clinical Radiology, https://doi.org/10.1016/j.crad.2022.08.148

round shape; the diffuse infiltrative type was defined as a tumour presenting with diffuse enlargement of the EOM or an ill-defined mass showing an amorphous shape. The signal intensity on T1-weighted images was classified as high if the signal intensity was equal to or higher than that of fat, intermediate if the signal intensity was lower than that of fat but equal to or higher than that of cerebral white matter, or low if the signal intensity was lower than that of cerebral white matter. On T2-weighted and fat-suppressed T2-weighted images, high was defined as a signal intensity equal to or higher than that of cerebrospinal fluid (CSF), intermediate was defined as lower than that of the CSF but equal to or higher than that of cerebral white matter, and low was defined as lower than that of cerebral white matter. For ADC measurements, the first two radiologists obtained mean ADC (ADC_{mean}) within the region of interest (ROI) on ADC maps. ROIs were determined as widely as possible while excluding the cystic portion by referring to morphological information on T2-weighted images with or without contrast-enhanced T1-weighted images. The average of the two radiologists' measurements was used as the final value.

Statistical analysis

Fisher's exact test was used to compare qualitative results (number of tumours, laterality, involved muscles, tumour morphology, signal intensities, and enhancement pattern). The Mann–Whitney *U*-test was used to compare the mean ADC values. Statistical significance was set at $p<0.05$. All statistical analyses were performed using EZR (Saitama Medical Center, Jichi Medical University, Shimotsuke, Japan), a graphical user interface for R (The R Foundation, The R Foundation for Statistical Computing, v. 2.13.0, Vienna, Austria).

Results

The clinical features of the 19 patients with EOM metastases are summarised in Table 1. The MRI features of EOM metastases and their comparison with those of other EOM diseases of non-thyroid origin are shown in Tables 2 and 3. Representative cases are presented in Figs 1–3.

Clinical features

Among the 19 patients, the most common primary tumour was breast cancer (n=13, 68%); other tumours included gastric cancer, rectal cancer, pancreatic cancer, thymus carcinoid, soft-tissue sarcoma, and vaginal melanoma. In one patient, EOM metastasis was an initial presentation of underlying malignancies; in the remaining patients, the mean and median times from primary diagnosis to EOM metastases were 7.6 and 3.4 years, respectively, with a range of 9–236 months. The most frequent symptom associated with EOM metastases was diplopia, occurring in seven patients; others included proptosis (n=3), reduced visual acuity or field (n=3), eye pain (n=2), ptosis (n=1), eyelid swelling (n=1); five patients showed no symptoms. All patients had metastases to other organs at the time they developed EOM metastases, including the bones (n=10), lung (n=8), brain (n=6), liver (n=5), and adrenal gland (n=4). Metastases to other skeletal muscles were found in only two patients.

Table 1
Clinical features in 19 patients with extraocular muscle (EOM) metastases.

Clinical features (n=19)	
Gender, *n* (%)	
Woman	17 (89)
Age (years, mean, range)	59.4 (20–82)
Primary tumour, *n* (%)	
Breast carcinoma	13 (68)
Others	6 (32)
Time interval from primary diagnosis to EOM metastases	
Initial presentation, *n* (%)	1 (5)
Duration of disease course, *n* (%)	18 (95)
Mean, median, range (month)	91, 41, 9–236
Presenting symptom, *n* (%)	
Diplopia	7 (37)
Proptosis	3 (16)
Reduced visual acuity or field	3 (16)
Eye pain	2 (11)
Eyelid swelling	1 (11)
Ptosis	1 (11)
None	5 (26)
Metastases to other organs, *n* (%)	
Present	19 (100)
Metastases to other muscles, *n* (%)	
Present	2 (11)

MRI features of EOM metastases

Of the 19 patients with EOM metastases, 10 patients had a single muscular involvement, and nine patients had multiple muscular involvement. Unilateral orbital involvement was observed in 14 patients, and bilateral orbital involvement was observed in five patients. Among the involved muscles, the inferior rectus muscle was the most commonly affected (29%), followed by the lateral rectus (25%), the medial rectus (22%), superior rectus (15%), and superior oblique (9%) muscles. The morphology classifications were focal discrete for nine patients and diffuse infiltrative for 10 patients. All the nine patients with focal discrete tumour presented with single muscular tumours, whereas nine of the 10 patients with diffuse infiltrative tumours had multimuscular tumours. On T1-weighted images, all tumours showed low or intermediate signal intensity. On T2-weighted images, the signal intensities were intermediate (n=13), a mixture of high and intermediate (n=4), and a mixture of intermediate and low (n=2). Fat-suppressed T2-weighted images were available for 13 patients, showing intermediate signal intensities in nine patients and a mixture of high and intermediate signals in four patients. Contrast-enhanced images were available for 14 patients and showed ring enhancement (n=5), heterogeneous

Please cite this article as: Miura A et al., MRI features of extraocular muscle metastases compared to those of other extraocular muscle diseases of non-thyroid origin, Clinical Radiology, https://doi.org/10.1016/j.crad.2022.08.148

Table 2
Summary of magnetic resonance imaging (MRI) features in 19 cases with extraocular muscle (EOM) metastases.

Case no	No.	Laterality	Involved muscles	Morphology	SI onT1WI	SI on T2WI	SI on fsT2WI	Enhancement	ADC_{mean} ($\times 10^{-3}mm^2/s$)
1	S	rt	rt-LR	Discrete	Inter	Inter	Inter	NA	1.1
2	S	lt	lt-IR	Discrete	Inter	Mix of high and inter	Mix of high and inter	Heterogeneous	0.55
3	S	rt	rt-SR	Discrete	Low	Inter	Inter	Ring	0.91
4	S	rt	rt-SO	Discrete	Low	Mix of high and inter	Mix of high and inter	NA	NA
5	S	rt	rt-MR	Discrete	Low	Inter	Inter	Heterogeneous	NA
6	S	rt	rt-IR	Discrete	Low	Mix of high and inter	Mix of high and inter	Ring	NA
7	S	rt	rt-LR	Discrete	Mix of inter and low	Mix of inter and low	Mix of high and inter	Heterogeneous	1.17
8	S	rt	rt-IR	Discrete	Inter	Inter	NA	Ring	NA
9	S	rt	rt-SR	Discrete	Low	Inter	Inter	Ring	NA
10	S	lt	lt-IR	Infiltrative	Low	Inter	Inter	Homogeneous	NA
11	M	lt	lt-IR, MR	Infiltrative	Inter	Inter	NA	Homogeneous	NA
12	M	bil	bil-LR, MR, IR, rt-SR	Infiltrative	Low	Inter	NA	Heterogeneous	0.91
13	M	bil	bil-LR, IR, lt-SR,MR, SO	Infiltrative	Low	Inter	Inter	Ring	0.89
14	M	bil	bil-LR	Infiltrative	Low	Inter	NA	Homogeneous	1.17
15	M	lt	lt-MR, SR, IR, SO	Infiltrative	Low	Low	Inter	Heterogeneous	NA
16	M	rt	rt-IR, MR, LR	Infiltrative	Low	Inter	Inter	NA	NA
17	M	bil	bil-LR, MR, SR, IR, SO	Infiltrative	Mix of inter and low	Mix of high and inter	NA	NA	0.84
18	M	bil	bil-IR, LR, MR, rt-IR	Infiltrative	Low	Inter	NA	NA	1.07
19	M	rt	rt-LR, MR, SR, IR, SO	Infiltrative	Low	Inter	Inter	Homogeneous	1.19

S, single; M, multiple; rt, right; lt, left; bil, bilateral; LR, lateral rectus; IR, inferior rectus; SR, superior rectus; SO, superior oblique; SI, signal intensity; fs, fat-supressed; Inter, intermediate; Mix, mixture; NA, not available, ADC; apparent diffusion coefficient.

Table 3
Comparison of magnetic resonance imaging features.

	EOM metastases (n=19)	Other diseases (n=24)	p-Value
No. of tumours			
Single	10 (53)	4 (17)	0.02
Multiple	9 (47)	20 (83)	
Laterality			
Unilateral	14 (74)	18 (75)	1.00
Bilateral	5 (26)	6 (25)	
Involved muscles	n=55	n=60	
Inferior rectus	16 (29)	12 (20)	0.28
Lateral rectus	14 (25)	16 (27)	1.00
Medial rectus	12 (22)	11 (18)	0.65
Superior rectus	8 (15)	17 (28)	0.11
Superior oblique	5 (9)	4 (7)	0.74
Morphology			
Discrete	9 (47)	0 (0)	<0.01
Infiltrative	10 (53)	24 (100)	
SI on T2WI			
Presence of hyperintensity	4 (21)	0 (0)	0.03
SI on FS T2WI	n=13	n=18	
Presence of hyperintensity	4 (31)	0 (0)	0.01
Enhancement pattern	n=14	n=7	
Ring or heterogeneous	10 (71)	0 (0)	< 0.01
Homogeneous	4 (29)	100 (100)	
ADC_{mean} ($\times 10^{-3}mm/^2s$)	n=10	n=8	
Mean, median	0.98, 0.99	0.96, 0.78	0.41

All categorical variables are expressed as n (%).
EOM, extraocular muscle; SI, signal intensity; FS, fat-suppressed; T2WI, T2-weighted imaging; ADC, apparent diffusion coefficient.

enhancement (n=5), and homogeneous enhancement (n=4). The mean and median ADC_{mean} values of the 10 tumours were 0.98 $\times$ 10^{-3} and 0.99 $\times$ 10^{-3} mm^2/s, respectively, ranging from 0.55 to 1.19 $\times$ 10^{-3} mm^2/s.

Comparison of MRI features between EOM metastases and other EOM diseases of non-thyroid origin

A single muscular presentation was significantly more common in EOM metastases group (p=0.02). There was no significant difference in the laterality or distribution of the involved muscles between the two groups (p=0.11 ~ 1.00). The discrete type of tumour morphology was significantly more common in the EOM metastases group (p<0.01). The signal intensities on T1-weighted images were low to intermediate in all cases in both groups. Hyperintense areas on T2-weighted or fat-suppressed T2-weighted images were observed only in the EOM metastases group (p=0.03, p=0.01). On contrast-enhanced T1-weighted images, ring or heterogeneous enhancement was observed only in the EOM metastases group (p<0.01). The ADC_{mean} did not differ significantly between the two groups (p=0.41).

Discussion

EOMs, despite their small volumes, are the third-most frequent site of muscle metastases, following the iliopsoas and gluteus muscles, and account for 91% of muscle

Please cite this article as: Miura A et al., MRI features of extraocular muscle metastases compared to those of other extraocular muscle diseases of non-thyroid origin, Clinical Radiology, https://doi.org/10.1016/j.crad.2022.08.148

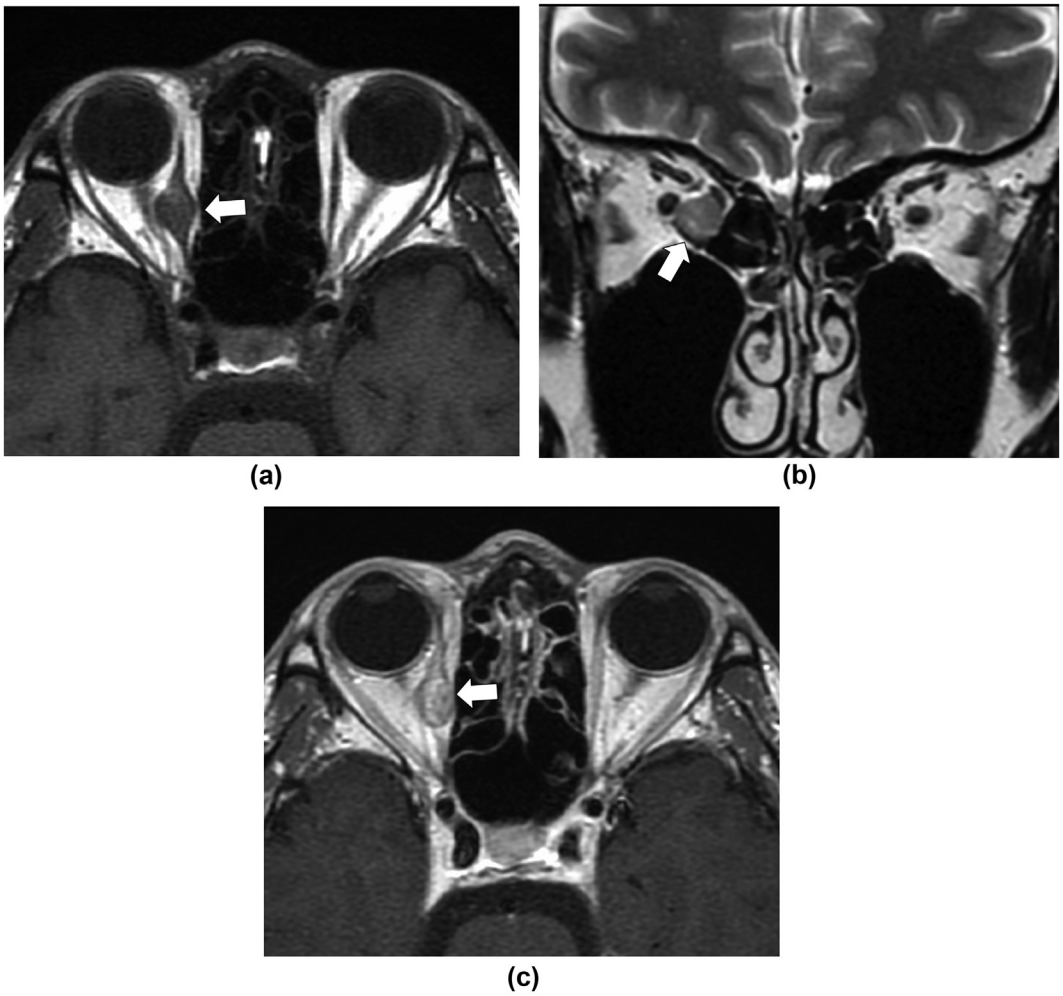

Figure 1 EOM metastases case 5 presents as a solitary discrete tumour. A 43-year-old woman developed EOM metastasis 9 years after the resection of a clear cell sarcoma of the ankle. (a) Axial T1-weighted image shows a discrete, well-defined mass in the right medial rectus muscle (arrow). (b) On the T2-weighted image, the mass shows intermediate signal intensity (arrow). (c) On the contrast-enhanced T1-weighted image, the tumour shows heterogeneous enhancement (arrow).

metastases in the head and neck region.[16] In the EOM metastases cases, all patients had distant metastases to other organs, suggesting a state of systemic carcinomatosis, but metastases to skeletal muscles other than EOMs were found in only two cases. This suggests that EOMs have a greater propensity for metastasis among the skeletal muscles, which might due to the EOM blood flow being more than 10-times greater than that of other skeletal muscles.[17] As another explanation, in terms of the seed and soil hypothesis,[18] it is postulated that some immunological mechanism or tumour cell adhesion factors specific for EOM may play a role in EOM metastases.[4,8]

Among the clinical features of EOM metastases cases, age distribution, variable presenting symptoms, variable time interval from the primary diagnoses, and usual concomitant metastases to other organs in the present series are consistent with EOM metastases data reviewed by Leung *et al.*[4] Breast cancer, melanomas, and carcinoids were reported to be the three most common primary tumours, but breast cancer was the only common primary tumour observed in the present patients. Related to this, a female-dominated sex distribution was observed in the present patients. This inconsistency may be attributed to the differences in cancer epidemiology between Japan and the Western countries that were the main data sources for the review of Leung *et al.*[4]

Among the involved muscles, the inferior rectus muscle was the most common in the present cases. This may reflect that Vmax, which is an indicator of vascularity defined as the maximum ratio of signal increase on dynamic contrast-enhanced MRI, is greatest in the inferior rectus muscle among the EOMs.[19] In contrast, the pooled data analysis by Leung *et al.* reported that the lateral rectus muscle was the most favourable site of EOM metastases.[4] This can be explained by the fact that the lacrimal artery, which feeds the lateral rectus muscle, has a greater diameter compared to those of muscular branches originating from the ophthalmic artery, which feed other EOMs.[4,20] These varying theories suggest that factors contributing to the distribution of EOM metastases are complex.

Please cite this article as: Miura A et al., MRI features of extraocular muscle metastases compared to those of other extraocular muscle diseases of non-thyroid origin, Clinical Radiology, https://doi.org/10.1016/j.crad.2022.08.148

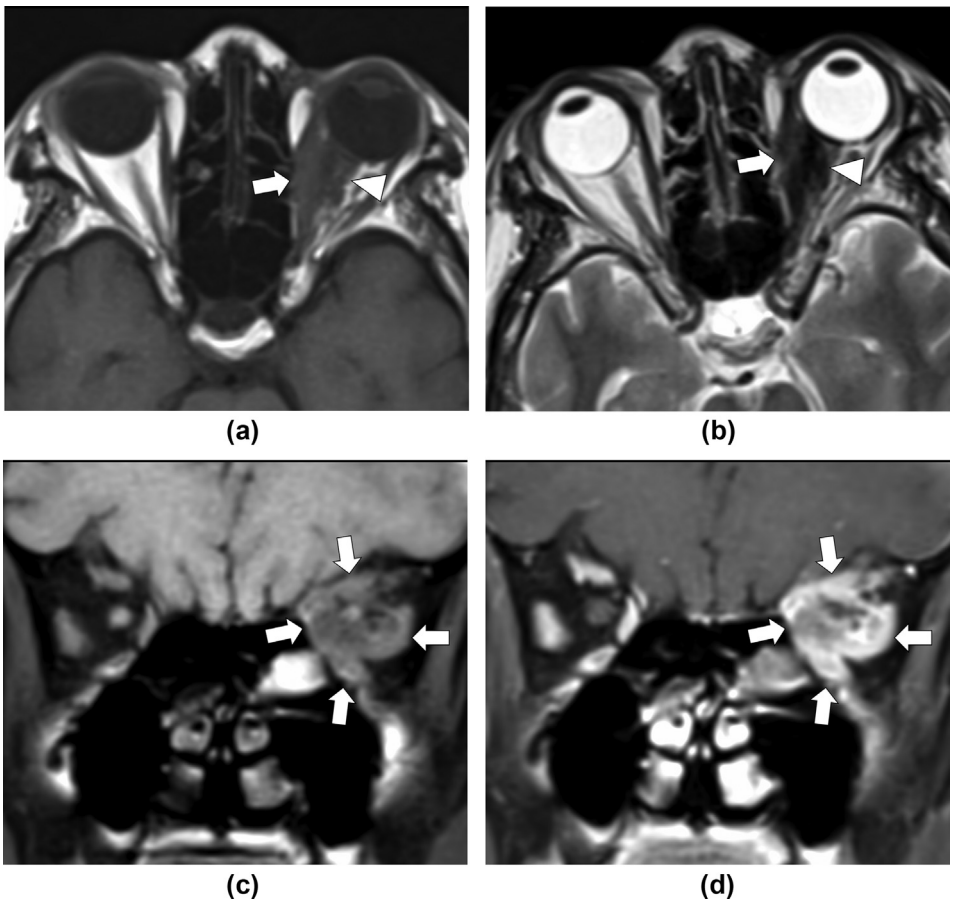

Figure 2 EOM metastases case 15 presents as multiple infiltrative tumours. A 63-year-old woman presented with diplopia and reduced visual acuity as a 10-year recurrence of gastric cancer. (a) Axial T1-weighted image shows an infiltrative mass in the left medial rectus muscle (arrow) and adjacent fat tissue (arrowhead). (b) On the T2-weighted image, the mass shows a mixture of intermediate and low intensities (arrow and arrowhead). (c,d) Coronal pre- and contrast-enhanced fat-suppressed T1-weighted images show multi-muscular involvement with heterogeneous enhancement (arrows).

The present study found that MRI images of EOM metastases showed two main patterns, a single discrete mass or multiple infiltrative masses, with the former pattern seeming to be specific features of EOM metastases. A discrete intramuscular mass is a common feature of metastases to other skeletal muscles, accounting for more than 70% of cases[21–23]; however, the specificity is low due to overlap with other conditions, including various soft-tissue tumours and abscesses.[21–23] In contrast, this feature was observed only in the EOM metastases cases in the present patients, which seems to reflect that soft-tissue tumours and abscesses originating from EOMs are rare.[1–3]

When EOM metastases manifest as multiple infiltrative masses, they mimic orbital lymphoma and other inflammatory diseases. The recognition of this pattern is important, because EOM metastases can occur in clinical situations where metastasis is not expected; this includes the initial presentation of an underlying malignancy or as a recurrence of malignancy delayed for >10 years.

In addition to focal discrete morphology, the present study suggests that the presence of hyperintensity on T2-weighted or fat-suppressed T2-weighted images, and ring or heterogeneous enhancement, would indicate EOM metastases rather than other diseases causing EOM enlargement. The presence of hyperintensity on T2-weighted images is thought to indicate central necrosis or the accumulation of secretory fluid, which are common histological features in metastatic tumours. In contrast, uniform lymphocyte infiltration is a histological feature common to orbital lymphoma and benign lymphoproliferative disorders,[24] which comprise the majority of the control group in this study. In agreement with the present results, EOM metastases cases have been reported with hyperintense areas on T2-weighted images,[7,8] whereas orbital lymphoma and benign lymphoproliferative disorders usually show low-to-intermediate signal intensity on T2-weighted images.[24,25]

Ring or heterogeneous enhancement is also thought to indicate central necrosis, accumulation of secretory fluid, or fibrosis in metastatic tumours. Although ring enhancements have been reported for 6–33% of skeletal muscle metastases other than EOM metastases,[21,23] the present study is the first to report that MRI images of EOM metastases can show ring enhancement. This can be explained by

Please cite this article as: Miura A et al., MRI features of extraocular muscle metastases compared to those of other extraocular muscle diseases of non-thyroid origin, Clinical Radiology, https://doi.org/10.1016/j.crad.2022.08.148

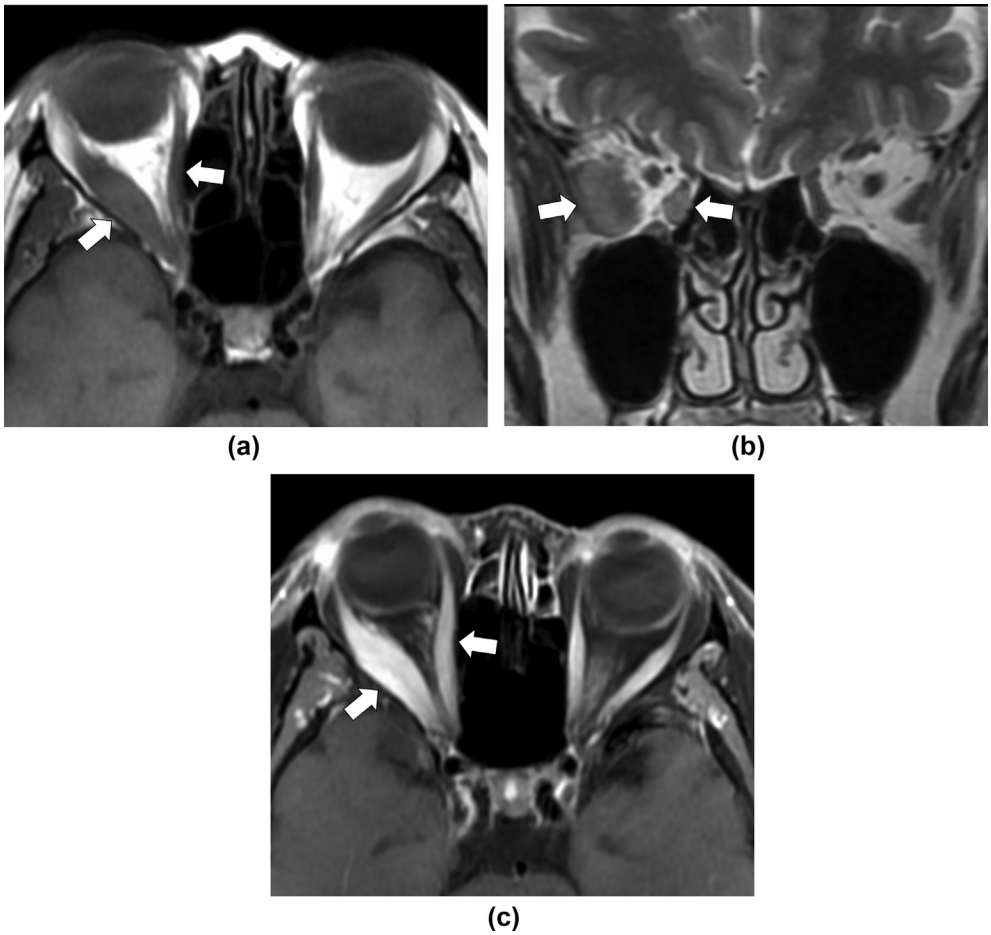

Figure 3 A 60-year-old man with idiopathic orbital inflammatory disease. (a,b) Axial T1-weighted and coronal T2-weighted images show diffuse enlargement of the right lateral and medial rectus muscles (arrows) with uniform intermediate signal intensities. (c) Contrast-enhanced fat-suppressed T1-weighted image shows homogeneous enhancement of the enlarged muscles (arrows).

the fact that previous studies on EOM metastases had only a few cases available for contrast-enhanced imaging. The present data on heterogeneous enhancement are consistent with previous reports, which suggested that heterogeneous enhancement could be used to differentiate between infiltrative metastases to skeletal muscle and myositis.[22]

The mean ADC values of malignant orbital tumours have been reported to be significantly lower than those of benign masses, with cut-off values ranging from 0.8 to 1.2×10^{-3} mm^2/s.[26–28] The mean ADC values in the present EOM metastases cases were nearly consistent with those of malignant orbital tumours; however, they were not helpful for differentiating between the EOM metastases and control groups. This might be explained by the fact that the control group consisted mainly of patients with lymphoproliferative diseases. Orbital lymphoproliferative diseases, whether benign or malignant, show restrictive diffusion coefficients,[24,25] with mean ADC values ranging from 0.5 to 1.1×10^{-3} mm^2/s; this is consistent with the present results.

This retrospective study has some limitations. First, the number of cases is relatively small, particularly in the control group, which includes a variety of diseases. Therefore, statistical differences may only have a complementary meaning. This is likely caused by the study design, which excluded thyroid-associated orbitopathy from the control group; however, this study design is appropriate for clinical practice, as thyroid-associated orbitopathy is diagnosed based on clinical features and laboratory findings rather than imaging findings. Second, conclusive histopathological diagnoses were obtained in only seven of the cases (37%); however, it may be difficult to collect a larger patient group with histological confirmation because of the low incidence of the disease and the impracticality of histological confirmation in patients with poor condition and/or disseminated malignancy status. Therefore, despite its limitations, the present case-series study to date can be considered meaningful.

In conclusion, EOM metastases can present as either a single discrete mass or multiple infiltrative masses. In addition to the former presentation, the presence of hyperintensity on T2-weighted images and ring or heterogeneous enhancement can be useful in differentiating EOM metastases from other EOM diseases.

Please cite this article as: Miura A et al., MRI features of extraocular muscle metastases compared to those of other extraocular muscle diseases of non-thyroid origin, Clinical Radiology, https://doi.org/10.1016/j.crad.2022.08.148

Declaration of competing interest

The author declares no conflict of interest.

References

1. Lacey B, Chang W, Rootman J. Nonthyroid causes of extraocular muscle disease. *Surv Ophthalmol* 1999;**44**:187–213.
2. Eade EL, Hardy TG, McKelvie PA, *et al*. Review of extraocular muscle biopsies and utility of biopsy in extraocular muscle enlargement. *Br J Ophthalmol* 2018;**102**:1586–90.
3. Savino G, Midena G, Tartaglione T, *et al*. Clinical–radiological patterns and histopathological outcomes in non-thyroid extraocular muscle enlargement: retrospective case series and current concepts. *Ophthalmic Plast Reconstr Surg* 2020;**36**:284–91.
4. Leung V, Wei M, Roberts TV. Metastasis to the extraocular muscles: a case report, literature review and pooled data analysis. *Clin Exp Ophthalmol* 2018;**46**:687–94.
5. Wladis EJ, Lee KW, Nazeer T. Metastases of systemic malignancies to the orbit: a major review. *Orbit* 2021;**40**:93–7.
6. Shields JA, Shields CL, Brotman HK, *et al*. Cancer metastatic to the orbit: the 2000 Robert M. Curts lecture. *Ophthalmic Plast Reconstr Surg* 2001;**17**:346–54.
7. Surov A, Behrmann C, Holzhausen HJ, *et al*. Lymphomas and metastases of the extra-ocular musculature. *Neuroradiology* 2011;**53**:909–16.
8. Gupta A, Chazen JL, Phillips CD. Carcinoid tumour metastases to the extraocular muscles: MR imaging and CT findings and review of the literature. *AJNR Am J Neuroradiol* 2011;**32**:1208–11.
9. Bonavolontà G, Strianese D, Grassi P, *et al*. An analysis of 2,480 space-occupying lesions of the orbit from 1976 to 2011. *Ophthalmic Plast Reconstr Surg* 2013;**29**:79–86.
10. Valenzuela AA, Archibald CW, Fleming B, *et al*. Orbital metastasis: clinical features, management and outcome. *Orbit* 2009;**28**:153–9.
11. Goldberg RA, Rootman J, Cline RA. Tumours metastatic to the orbit: a changing picture. *Surv Ophthalmol* 1990;**35**:1–24.
12. Ahmad SM, Esmaeli B. Metastatic tumours of the orbit and ocular adnexa. *Curr Opin Ophthalmol* 2007;**18**:405–13.
13. Alsuhaibani AH, Nerad JA. Thyroid-associated orbitopathy. *Semin Plast Surg* 2007;**21**:65–73.
14. Bartley GB, Gorman CA. Diagnostic criteria for Graves' ophthalmopathy. *Am J Ophthalmol* 1995;**119**:792–5.
15. Surov A, Hainz M, Holzhausen HJ, *et al*. Skeletal muscle metastases: primary tumours, prevalence, and radiological features. *Eur Radiol* 2010;**20**:649–58.
16. Lupi A, Weber M, Del Fiore P, *et al*. The role of radiological and hybrid imaging for muscle metastases: a systematic review. *Eur Radiol* 2020;**30**:2209–19.
17. Wilcox Jr LM, Keough EM, Connolly RJ, *et al*. Comparative extraocular muscle blood flow. *J Exp Zool* 1981;**215**:87–90.
18. Amerasekera S, Turner M, Purushotham AD. Paget's "seed and soil" hypothesis revisited. *J BUON* 2004;**9**:465–7.
19. Taoka T, Iwasaki S, Uchida H, *et al*. Enhancement pattern of normal extraocular muscles in dynamic contrast-enhanced MR imaging with fat suppression. *Acta Radiol* 2000;**41**:211–6.
20. Aydin A, Cakir A, Ersanli D. Isolated extraocular muscle involvement as the ophthalmic manifestation of leukaemia: an alternative explanation. *Clin Exp Ophthalmol* 2010;**38**:651.
21. Surov A, Fiedler E, Voigt W, *et al*. Magnetic resonance imaging of intramuscular metastases. *Skeletal Radiol* 2011;**40**:439–46.
22. Soliman F, Hwang S, Landa J, *et al*. Infiltrative pattern of carcinomatosis in extremity muscles on MRI. *Clin Imaging* 2016;**40**:451–5.
23. Surov A, Hainz M, Holzhausen HJ, *et al*. Skeletal muscle metastases: primary tumours, prevalence, and radiological features. *Eur Radiol* 2010;**20**:649–58.
24. Haradome K, Haradome H, Usui Y, *et al*. Orbital lymphoproliferative disorders (OLPDs): value of MR imaging for differentiating orbital lymphoma from benign OPLDs. *AJNR Am J Neuroradiol* 2014;**35**:1976–82.
25. Sun B, Song L, Wang X, *et al*. Lymphoma and inflammation in the orbit: diagnostic performance with diffusion-weighted imaging and dynamic contrast enhanced MRI. *J Magn Reson Imaging* 2017;**45**:1438–45.
26. Ro SR, Asbach P, Siebert E, *et al*. Characterization of orbital masses by multiparametric MRI. *Eur J Radiol* 2016;**85**:324–36.
27. Xu XQ, Qian W, Ma G, *et al*. Combined diffusion-weighted imaging and dynamic contrast-enhanced MRI for differentiating radiologically indeterminate malignant from benign orbital masses. *Clin Radiol* 2017;**72**:903.e9.
28. Xu XQ, Hu H, Su GY, *et al*. Diffusion weighted imaging for differentiating benign from malignant orbital tumours: diagnostic performance of the apparent diffusion coefficient based on region of interest selection method. *Korean J Radiol* 2016;**17**:650–6.

Please cite this article as: Miura A et al., MRI features of extraocular muscle metastases compared to those of other extraocular muscle diseases of non-thyroid origin, Clinical Radiology, https://doi.org/10.1016/j.crad.2022.08.148